Electronic Supplementary Material (ESI) for Materials Chemistry Frontiers.

Supporting Information

Robust imidazole-linked Ni-phthalocyanine-based covalent-organic framework four CO_2 electroreduction in full pH range

Xu Yang,[a,c], Duan-Hui Si,[a*] Hong-Fang Li,[a] Rong Cao[a,b,d*] and Yuan-Biao Huang[a,b,d*]

[a] Prof. D.-H. Si, Prof. Y.-B. Huang, Prof. R. Cao, X. Yang, Prof. H.-F. Li

State Key Laboratory of Structural Chemistry

Fujian Institute of Research on the Structure of Matter, Chinese Academy of Sciences

Fuzhou 350002, China

[b] Prof. Y.-B. Huang, Prof. R. Cao

Fujian Science & Technology Innovation Laboratory for Optoelectronic Information of China

Fuzhou, Fujian, 350108, P. R. China

Fuzhou 350108, China

[c] X. Yang

Fujian Cross Strait Institute of Flexible Electronics (Future Technology), Fujian Normal University

Fuzhou, 350117, China

[d] Prof. Y.-B. Huang, Prof. R. Cao

University of Chinese Academy of Sciences

Beijing 100049, China

E-mail: ybhuang@fjirsm.ac.cn; rcao@fjirsm.ac.cn

1. Materials and Synthetic Procedures:

1.1. Materials

All solvents, reagents and chemicals were purchased from commercial suppliers, such as Sigma-Aldrich, TCI and J&K and used without further purification unless specially addressed. All aqueous solutions were prepared with Ultrapure water (18.25 MΩ·cm).

1.2. Monomer synthesis

NiPc-$(NH_2)_8$ was synthesized following a literature procedure.[1]

1.3. The synthesis of NiPc-Im-COF

NiPc-Im-COF was prepared as follows. A Pyrex tube measuring 10×8 mm (o.d × i.d) was charged with NiPc-$(NH_2)_8$ (13.80 mg, 0.02 mmol), BPDH (5.4 mg, 0.04 mmol), NMP/mesitylene (1.2 mL/0.3 mL). After sonication for 30 minutes, the tube was flash frozen at 77 K (liquid N_2 bath). After one freeze-pump-thaw cycle the tube was flame sealed under vacuum. Upon sealed, the length of the tube was reduced to approximately 12 cm. The reaction was heated at 170 ºC for six days. After cooling to room temperature, the dark green solid was collected by centrifugation and washed with *N,N′*-dimethylformamide and dichloromethane. Finally, the product was evacuated at 70 ºC overnight to give NiPc-Im-COF as dark green powder.

2. Methods

2.1. Characterization

Powder X-ray diffraction (PXRD) patterns were recorded on a Miniflex-600 diffractometer using Cu Kα radiation (λ = 0.154 nm). Fourier transform infrared (FT-IR) spectroscopy was performed using KBr pellets on a Bruker VERTEX70 spectrometer in the 400-4000 cm^{-1}. Solid-state ^{13}C NMR spectra of COF was recorded on Bruker-Biospin AVANCE Ⅲ HD spectrometer. X-ray photoelectron spectroscopy

(XPS) measurements were performed on an ESCALAB 250Xi X-ray photoelectron spectrometer (Thermo Fisher) using an Al Ka source (15 kV, 10 mA). (the C-C peak here were corrected to 284.8 eV). Elemental analyses (EA) of C, H, and N were carried out on an Elementar Vario EL-Cube analyzer. Thermogravimetric analysis (TGA) were performed under a nitrogen atmosphere with a heating rate of 5 ºC min^{-1} by using an SDT Q600 thermogravimetric analyser. The content of Ni in the solid samples was detected by inductively coupled plasma atomic emission spectroscopy (ICP-AES) on an Ultima2 analyzer (Jobin Yvon). Scanning electron microscopy (SEM) images were obtained by field emission scanning electron microscopy (JSM6700-F). Transmission electron microscope (TEM) images were recorded by a ThermoFisher Scientific TALOS F200X G2 working at 200 kV. N_2 adsorption-desorption isotherm and the Brunauer-Emmett-Teller (BET) surface area measurements were measured by using Micromeritics ASAP 2460 instrument. CO_2 sorption isotherm was measured by using Micrometrics ASAP 2020 instrument. The gas chromatography measurements were performed on the Agilent 7820A gas chromatograph (GC) equipped with FID and TCD.

2.2. Activation of Im-COF before BET measurement

The isolated powders was transferred to a Soxhlet extractor and thoroughly washed with DCM (24 h) and THF (24 h). Following that, the product was thoroughly washed with liquid CO_2. The system was then heated up to 45 ºC to bring about the supercritical state of CO_2 and slowly bled to ambient pressure. Finally the product of NiPc-Im-COF was degassed at room temperature for 10 h at 10^{-2} mTorr to yield activated sample.

2.3. Electrochemical measurements

2.3.1 CO2RR test in H-cell

Electrochemical experiments were implemented in a designed H-type electrochemical cell with two compartments separated by anion-exchange membrane (Nafion-117). Each compartment contained 70 mL electrolyte (0.5 M $KHCO_3$ made from ultrapure water). The working electrode was fabricated by coating 60 μL catalyst ink into carbon fiber paper electrode with 1 cm ×1 cm. The homogeneous ink was prepared using 5 mg of catalyst and 2 mg ketjenblack dispersed into 1 mL of isopropanol containing 50 μL Nafion solution (5 wt%). Electrochemical measurements were performed in a three-electrode cell using the Ag/AgCl electrode as the reference electrode and Pt guaze as the counter electrode. Before the CO_2 electrochemical reduction, the electrolyte in the cathodic compartment was purged with CO_2 gas for at least 30 min to achieve the CO_2-saturated solution (pH = 7.3). Cyclic voltammetry (CV) experiments were conducted at room temperature at 100 mV s^{-1}. Linear sweep voltammetry (LSV) was performed with a scan rate of 10 mV s^{-1} from -0.62 to -1.82 V vs. Ag/AgCl in CO_2-saturated 0.5 M $KHCO_3$ electrolyte. In the studies, all potentials were converted to potential vs. reversible hydrogen electrode (RHE) according to the equation E (vs. RHE) = E (vs. Ag/AgCl) + 0.1989 V + 0.059 × pH. CO_2 gas was delivered at an average rate of 30 mL·min^{-1} (at room temperature and ambient pressure) and routed into the gas sampling loop (0.8 mL) of a gas chromatograph. The gas phase composition was analyzed by GC every 15 min. The separated gas products were analyzed by a thermal conductivity detector (for H_2) and a flame ionization detector (for CO).

2.3.2 CO_2RR test in Flow cell

Electrochemical measurements with high current densities were performed in a flow cell consists of a gas diffusion electrode (GDE), an anion exchange membrane and a carbon paper gas diffusion layer (GDL) anode. 100 μL catalyst ink was loaded onto a 0.8 cm^2 GDL to create a GDE. The homogeneous ink was prepared using 5 mg of catalyst and 2 mg ketjenblack dispersed into 1 mL of isopropanol containing 50 μL Nafion solution (5 wt%). An Ag/AgCl was acted as the reference. 1 M, 3 M and 5 M KOH aqueous solution was used as electrolyte and was circulated through the anode side using a peristaltic pump. CO_2 gas was supplied to the cathode side with a constant flow rate of 20 (sccm) ml min^{-1} monitored by a flow controller. Linear sweep voltammetry (LSV) was performed with a scan rate of 10 mV s^{-1} from -0.6 to -1.8 V vs. Ag/AgCl. In the studies, all potentials were converted to potential vs. reversible hydrogen electrode (RHE) according to the equation E (vs. RHE) = E (vs. Ag/AgCl) + 0.1989 V + 0.059 × pH. During electrolysis procedure, the effluent gas from the cathode compartment went through the sampling loop (0.8 mL) of a gas chromatograph. The gas phase composition was analyzed by GC every 15 min. The separated gas products were analyzed by a thermal conductivity detector (for H_2) and a flame ionization detector (for CO).

Faradaic efficiency:

The Faradaic efficiency (FE) for CO production at each applied potential was calculated based on the following equations:

$$FE = \frac{J_{CO}}{J_{total}} = \frac{\upsilon_{CO} \times N \times F}{J_{total}}$$

FE: Faradaic efficiency for CO production;

J_{CO}: partial current density for CO production;

J_{total}: total current density;

$\upsilon_{CO:}$ the production rate of CO (measured by GC);

N: the number of electron transferred for product formation, in which it is 2 for CO;

F: Faradaic constant, 96485 C mol^{-1}.

Turnover Frequency (TOF, h^{-1}):

The TOF for CO was calculated based on the following equations:

$$TOF = \frac{I_{product} / NF}{m_{cat} \times \omega / M_{metal}} \times 3600$$

$I_{product}$: partial current for certain product, CO;

N: the number of electron transferred for product formation, in which it is 2 for CO;

F: Faradaic constant, 96485 C mol^{-1};

m_{cat}: catalyst mass in the electrode, g;

ω: metal loading in the catalyst;

M_{metal}: atomic mass of metal, g mol^{-1} .

2.4 Computational methods

All calculations on NiPc-Im-COF in this study were performed with Vienna Ab initio Simulation Package (VASP)[2-5], which were considered with Perdew-Burke-Ernzerh (PBE)flavor[6] of density functional theory (DFT) and the Projector Augmented Wave

(PAW)method.[7, 8] The cutoff energy of plane wave basis and the convergence criteria were set to 450 eV and 1×10^{-5} eV respectively. A k-point sampling of (2,2,1) was used. The clusters areseparated from their periodic images in all directions by a vacuum space of 20 Å.

3. Figures and Tables

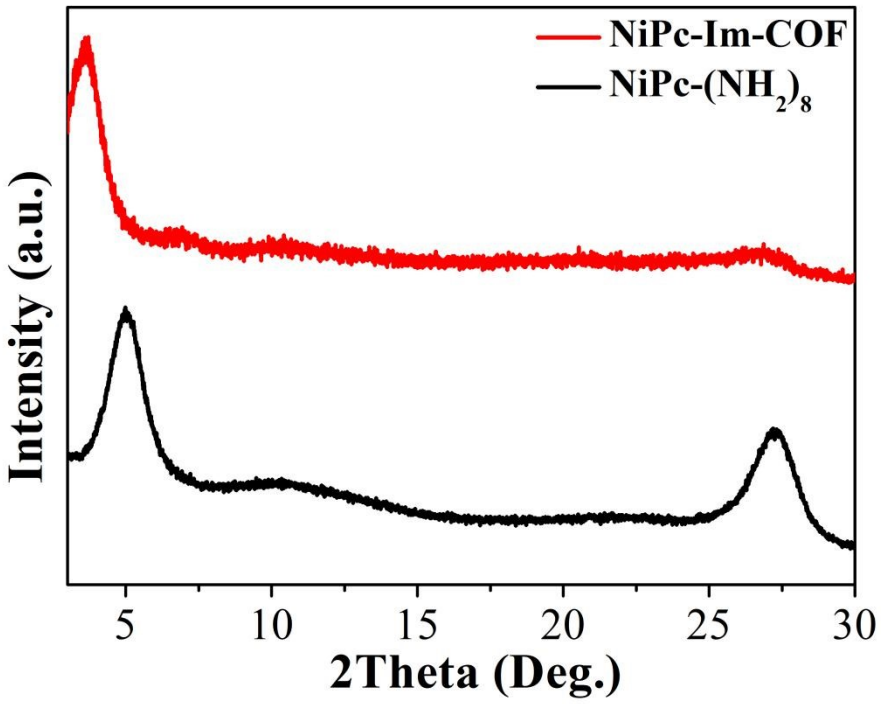

Figure S1. PXRD of NiPc-$(NH_2)_8$ and NiPc-Im-COF. The main peaks of NiPc-$(NH_2)_8$ were located at 5.02° and 27.3°, which were different from that of NiPc-Im-COF.

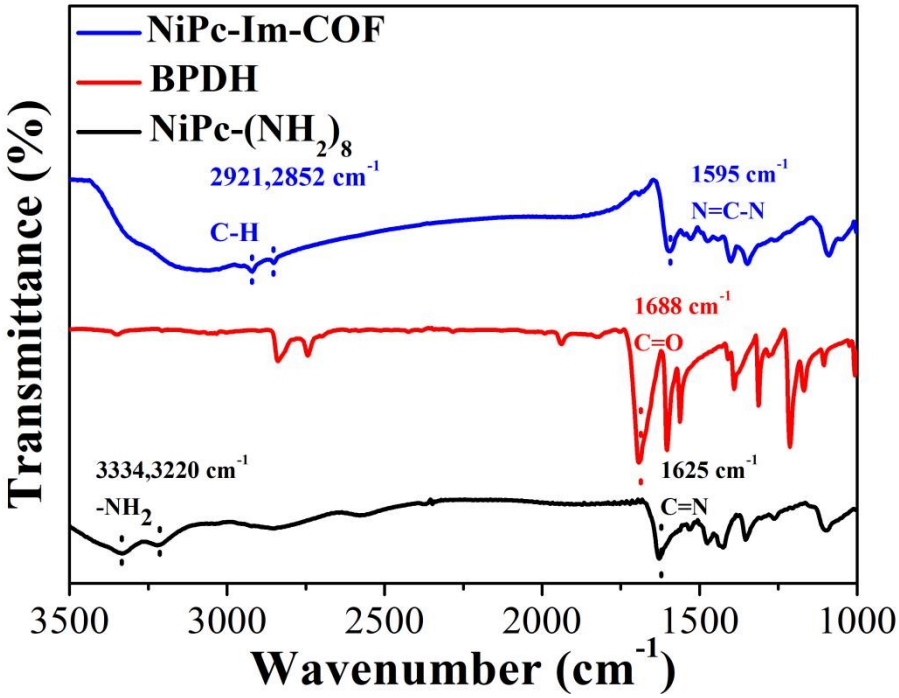

Figure S2. IR of NiPc-$(NH_2)_8$, BPDH and NiPc-Im-COF.

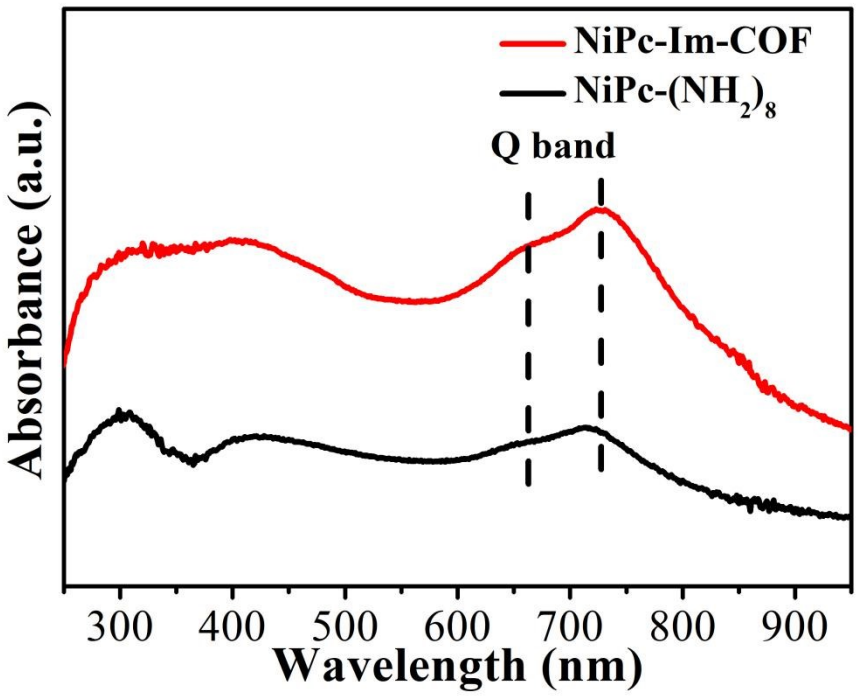

Figure S3. UV-Vis spectra of NiPc-Im-COF and NiPc-$(NH_2)_8$.

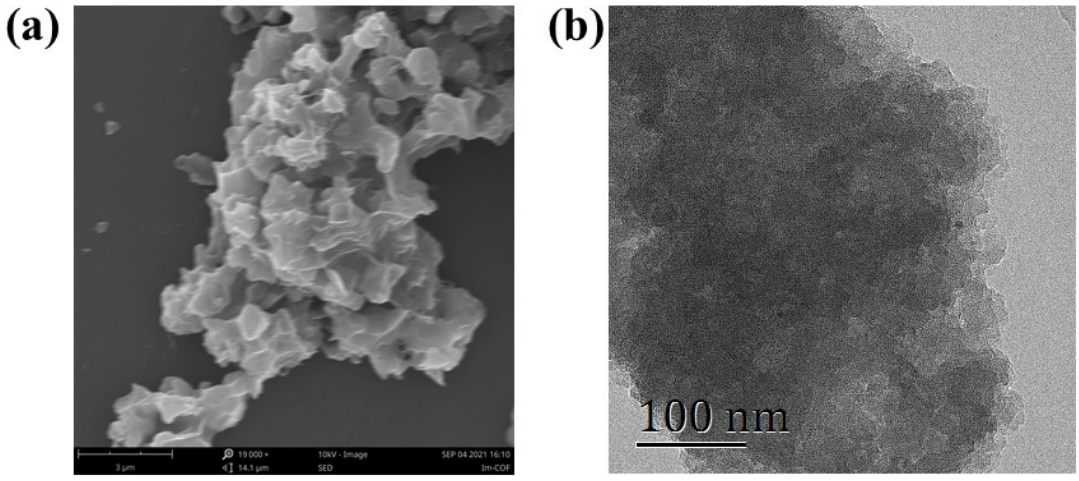

Figure S4. (a) SEM and (b) TEM of NiPc-Im-COF.

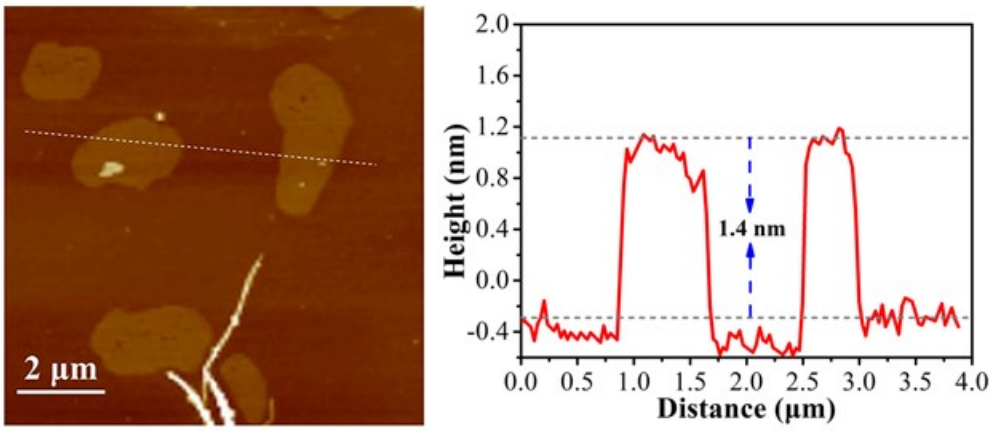

Figure S5. (a) AFM image and (b) height of NiPc-Im-COF.

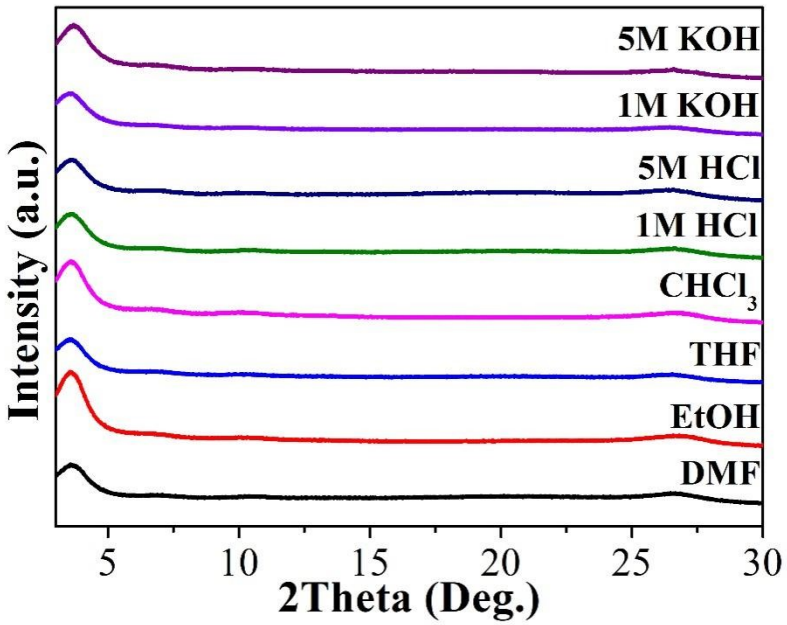

Figure S6. The chemical stability of NiPc-Im-COF tested in DMF, EtOH, THF, $CHCl_3$, 1 and 5 M HCl and 1 and 5 M KOH at room temperature.

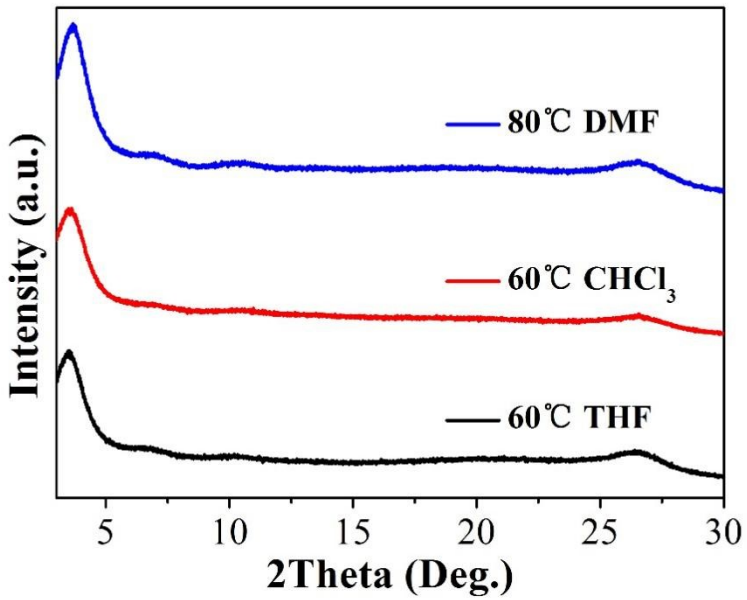

Figure S7. The chemical stability of NiPc-Im-COF tested in DMF, THF and $CHCl_3$ at 80 °C and 60 °C.

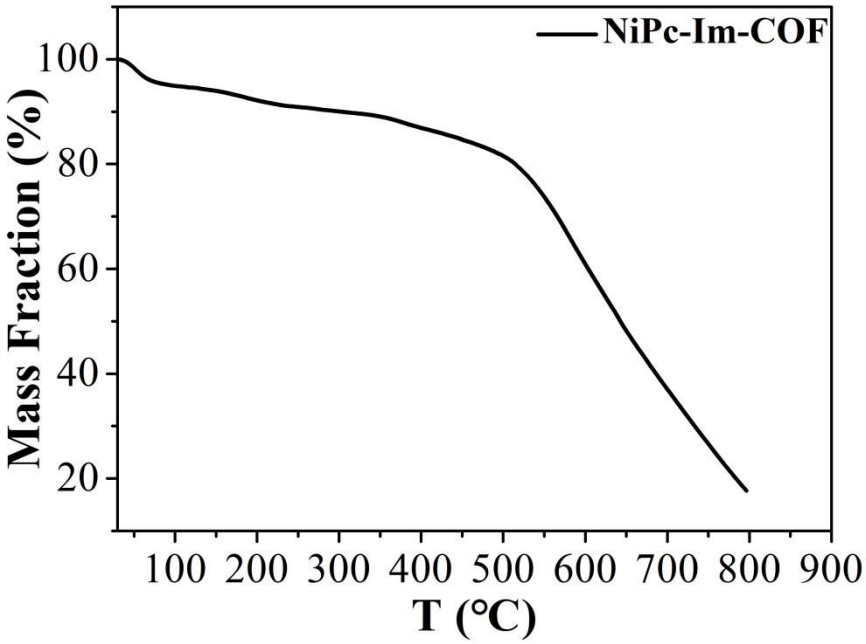

Figure S8. TGA curve of NiPc-Im-COF.

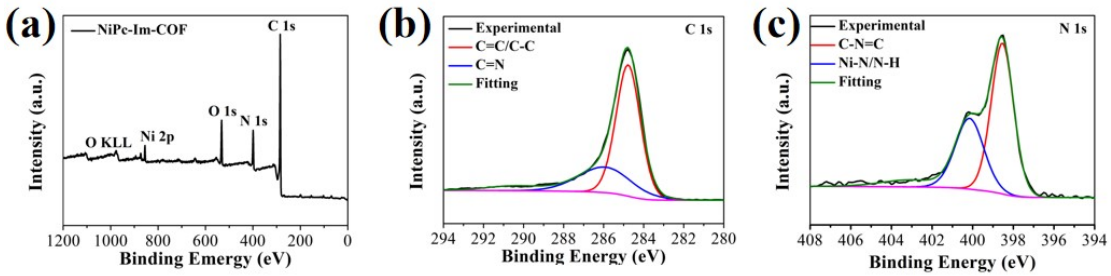

Figure S9. (a) Survey, (b) C 1S and (c) N 1s XPS spectra of NiPc-Im-COF.

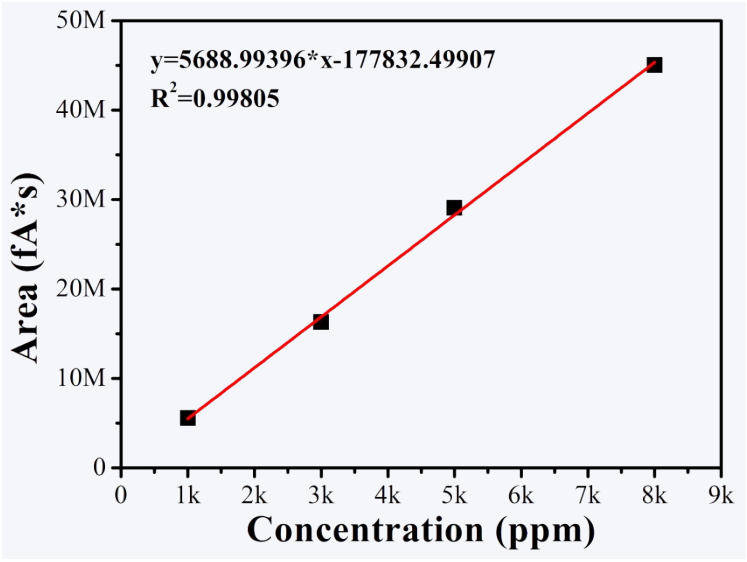

Figure S10. The calibration curve of CO.

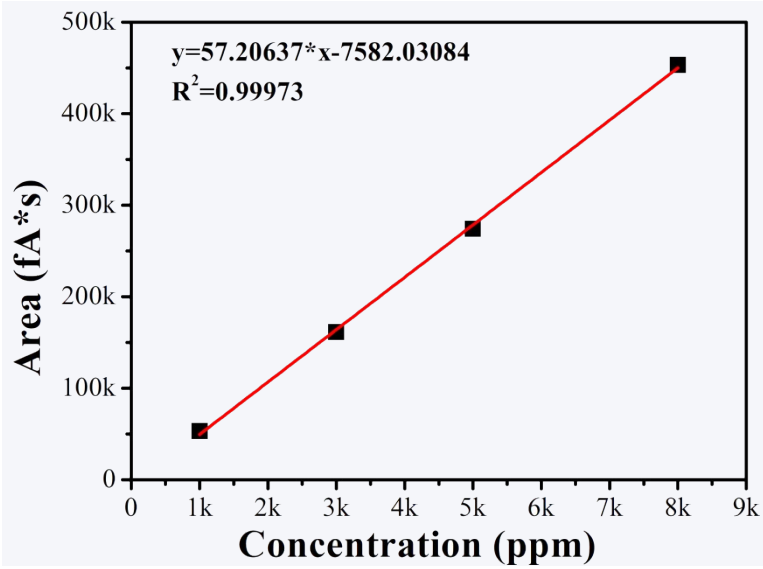

Figure S11. The calibration curve of H_2.

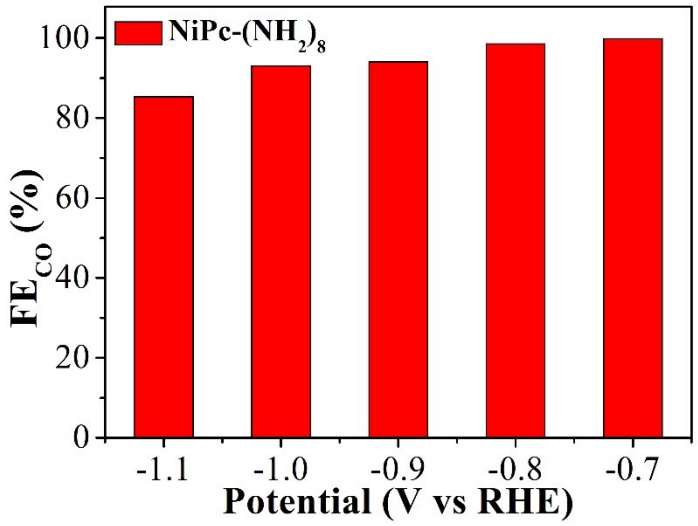

Figure S12. FECO in 0.5 M $KHCO_3$ of NiPc-$(NH_2)_8$.

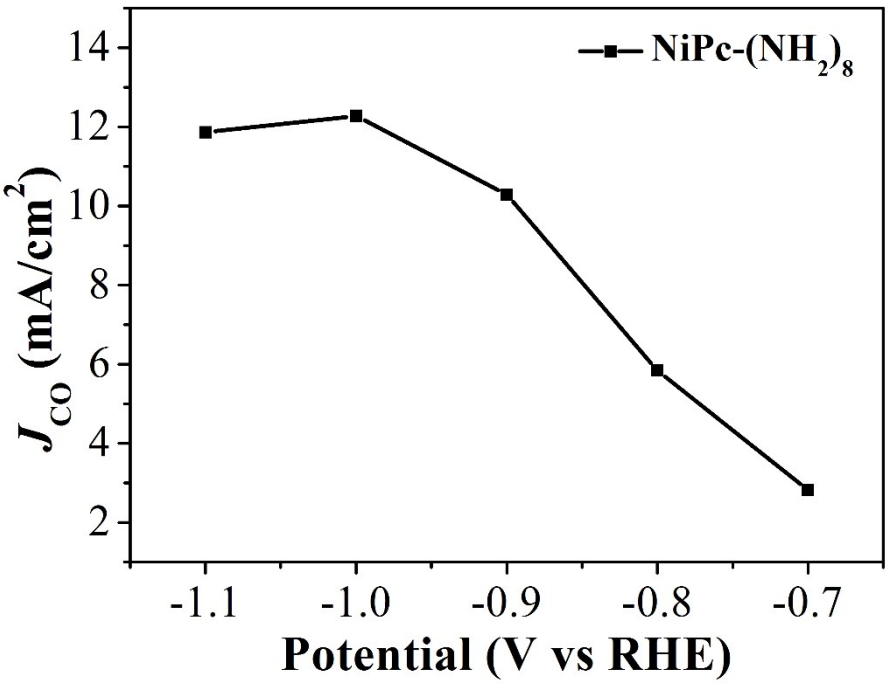

Figure S13. CO partial current density in 0.5 M $KHCO_3$ of NiPc-$(NH_2)_8$.

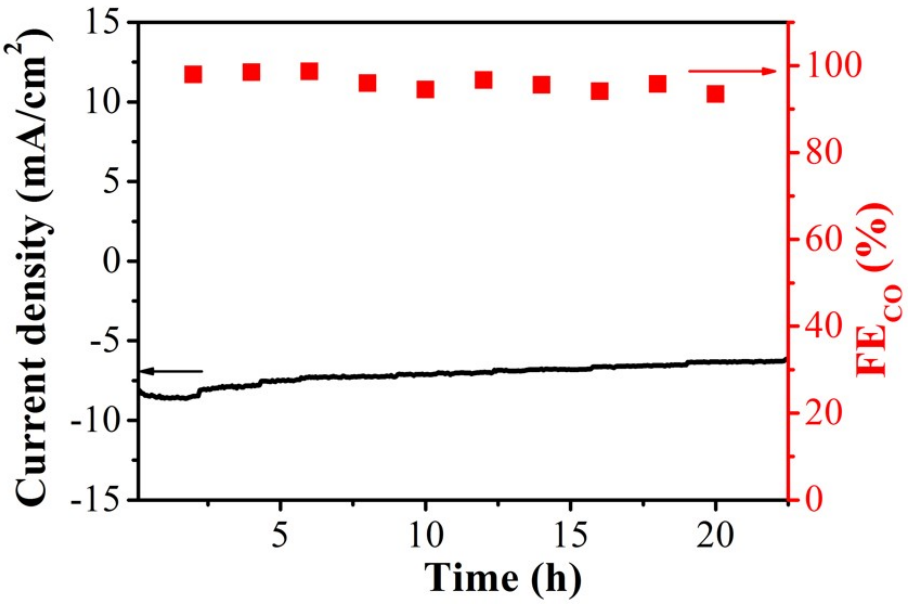

Figure S14. Long time stability test of NiPc-Im-COF at -0.8 V vs RHE in H-cell with 0.5 M $KHCO_3$ as electrolyte.

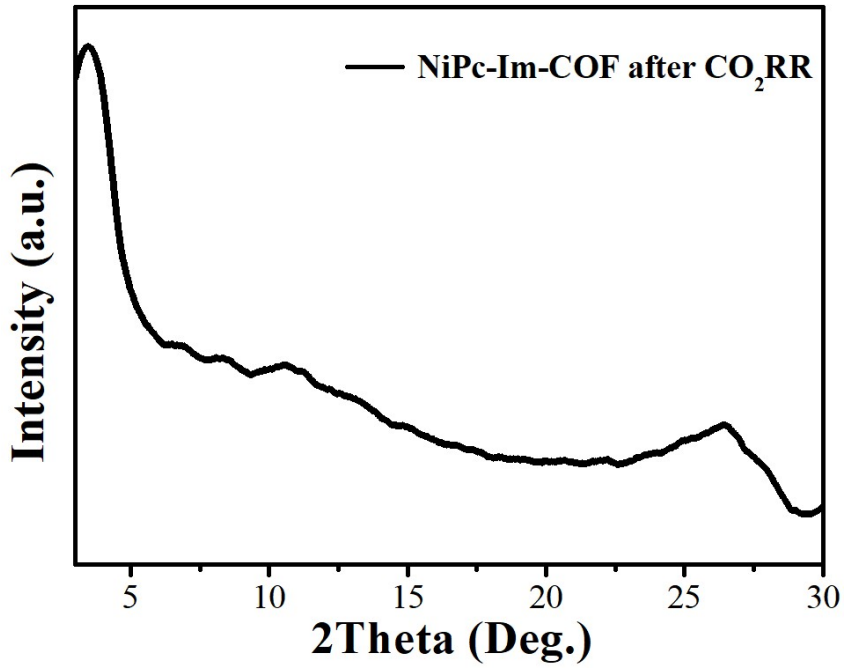

Figure S15. PXRD pattern of NiPc-Im-COF after electrocatalytic CO_2RR in 0.5 M $KHCO_3$.

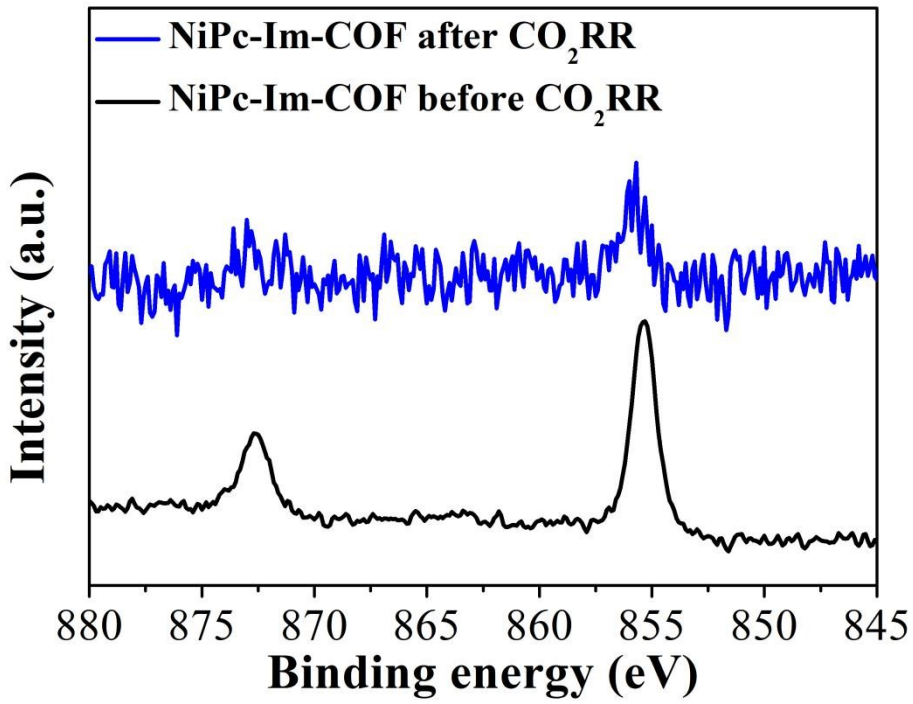

Figure S16. High-resolution Ni 2p XPS spectrum of NiPc-Im-COF before and after CO_2RR testing in H-cell with 0.5 M $KHCO_3$ as electrolyte.

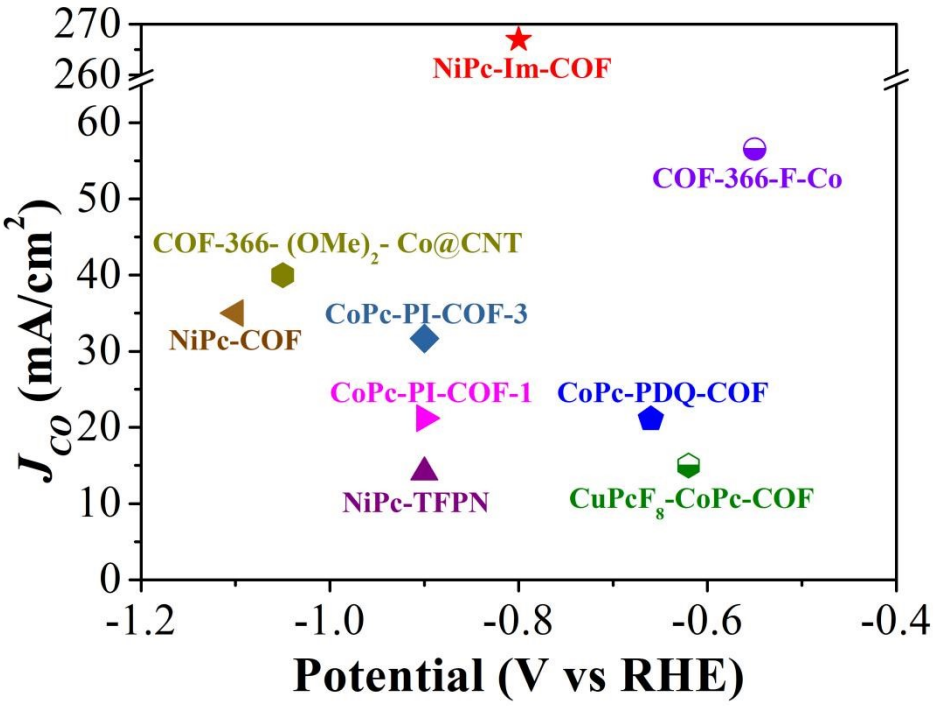

Figure S17. The comparison of J_{CO}.

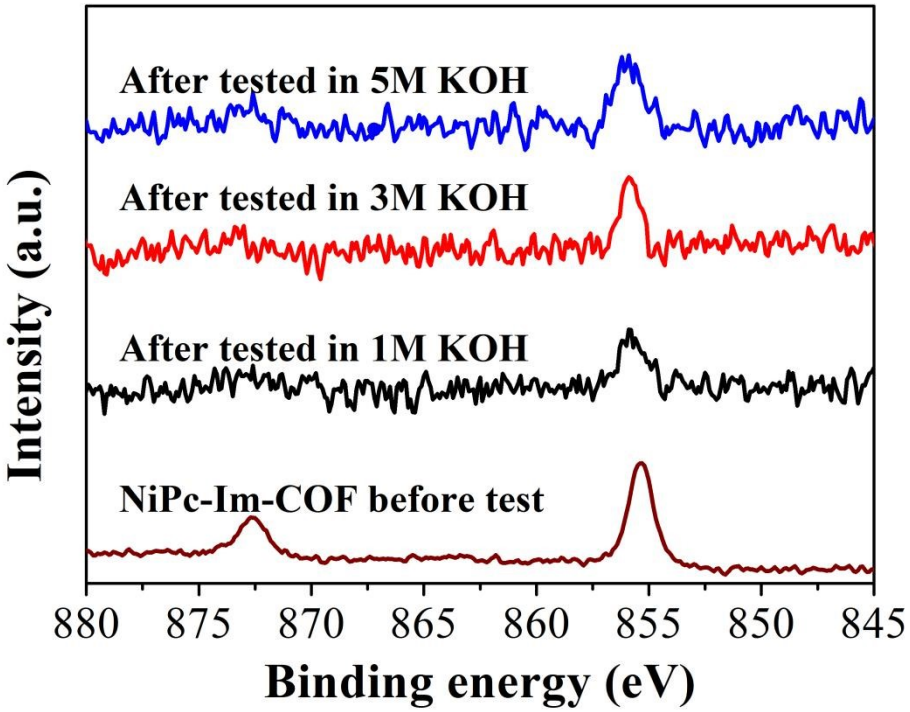

Figure S18. High-resolution Ni 2p XPS spectrum of NiPc-Im-COF before and after CO_2RR testing in GDE with 1 M, 3 M and 5 M KOH as electrolyte.

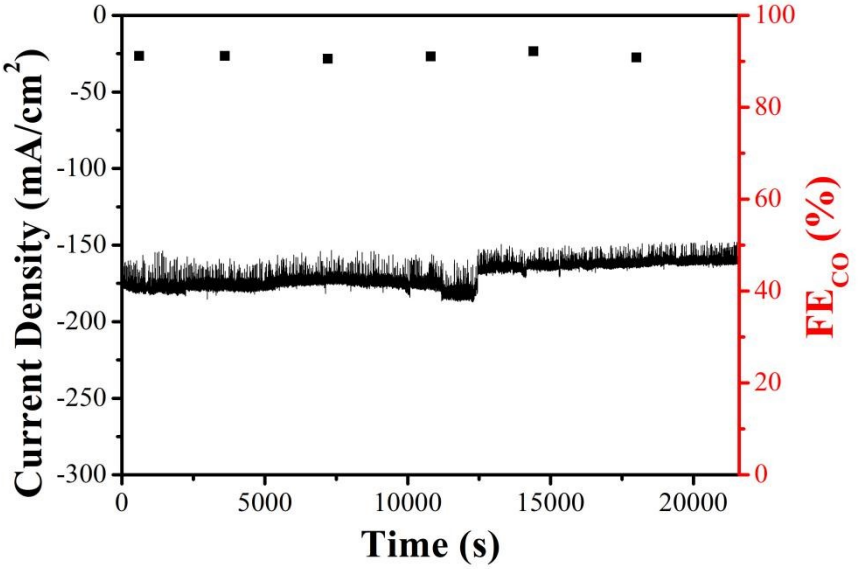

Figure S19. Long time stability test of NiPc-Im-COF at -0.6 V vs RHE in GDE with 5 M KOH as electrolyte.

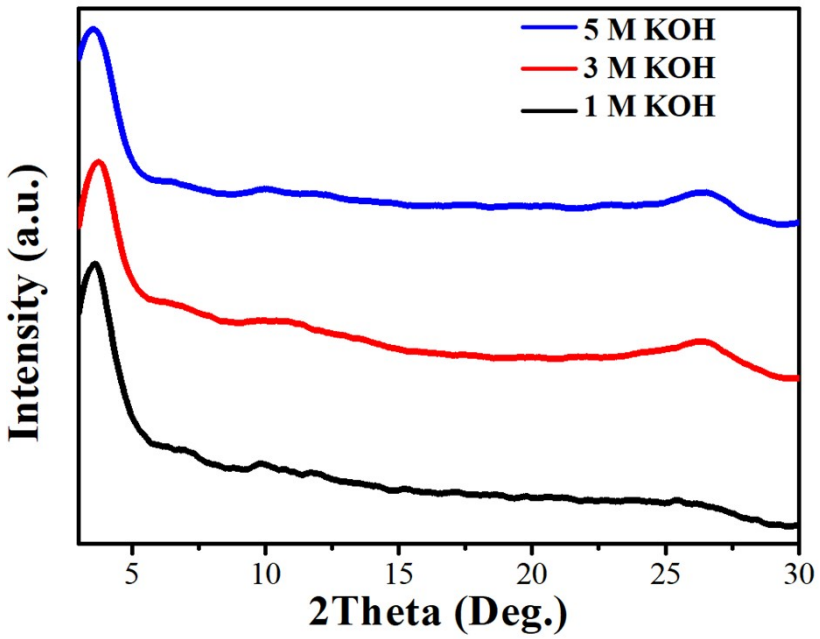

Figure S20. PXRD pattern of NiPc-Im-COF after electrocatalytic CO_2RR in different concentration KOH.

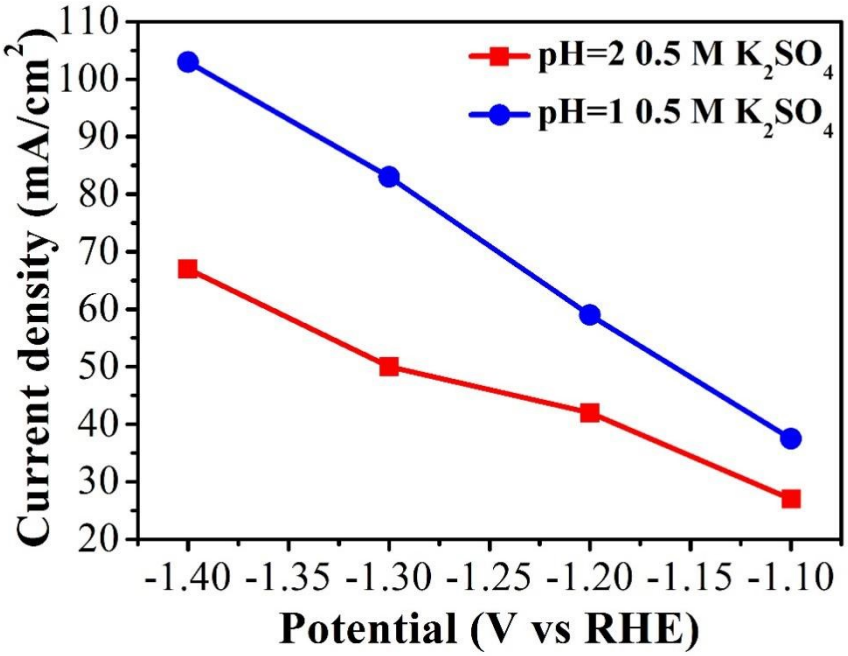

Figure S21. The total current density at different potentials in 0.5 M K_2SO_4 (pH=1 and 2).

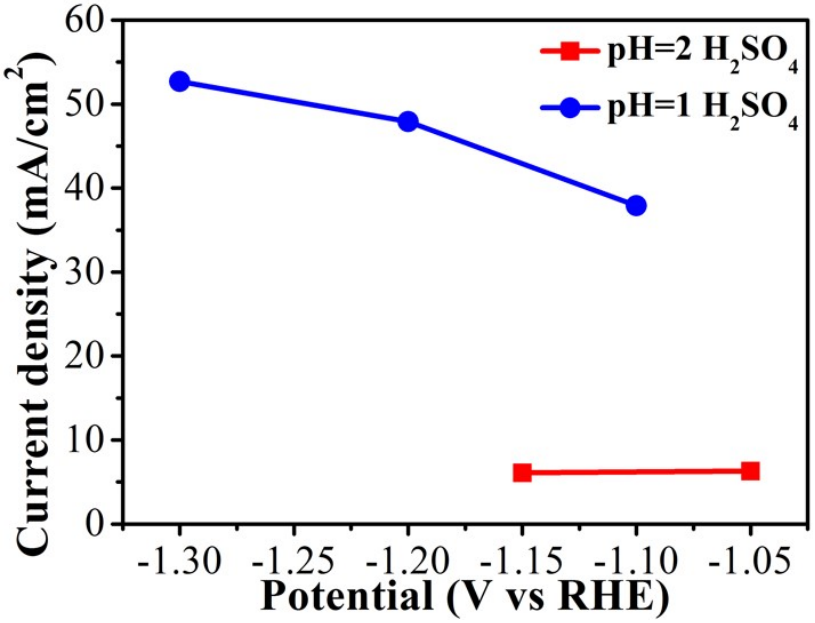

Figure S22. The total current density at different potentials in H_2SO_4 (pH=1 and 2).

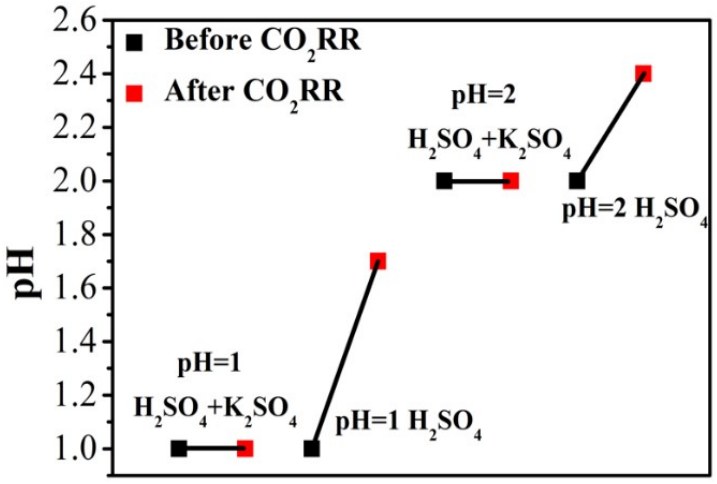

Figure S23. pH values before and after the CO_2RR of different electrolytes.

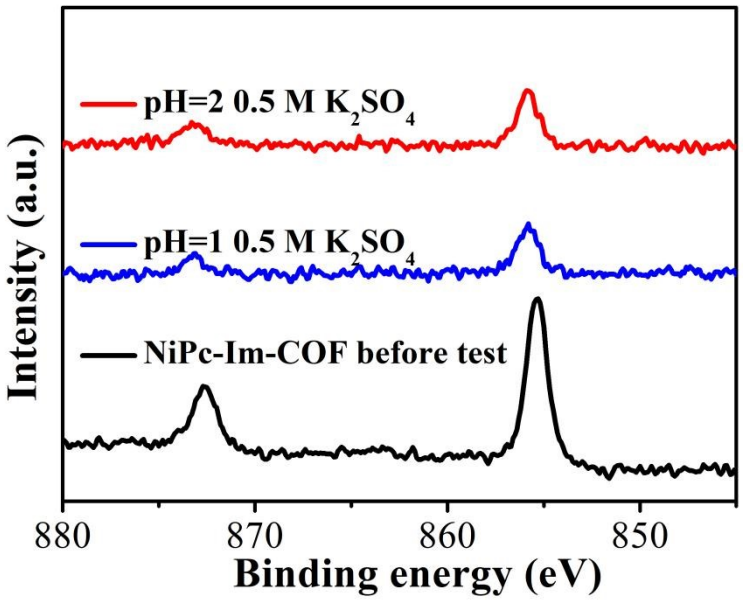

Figure S24. High-resolution Ni 2p XPS spectrum of NiPc-Im-COF before and after CO_2RR testing in GDE with 0.5 M K_2SO_4 (pH=1 and 2) as electrolyte.

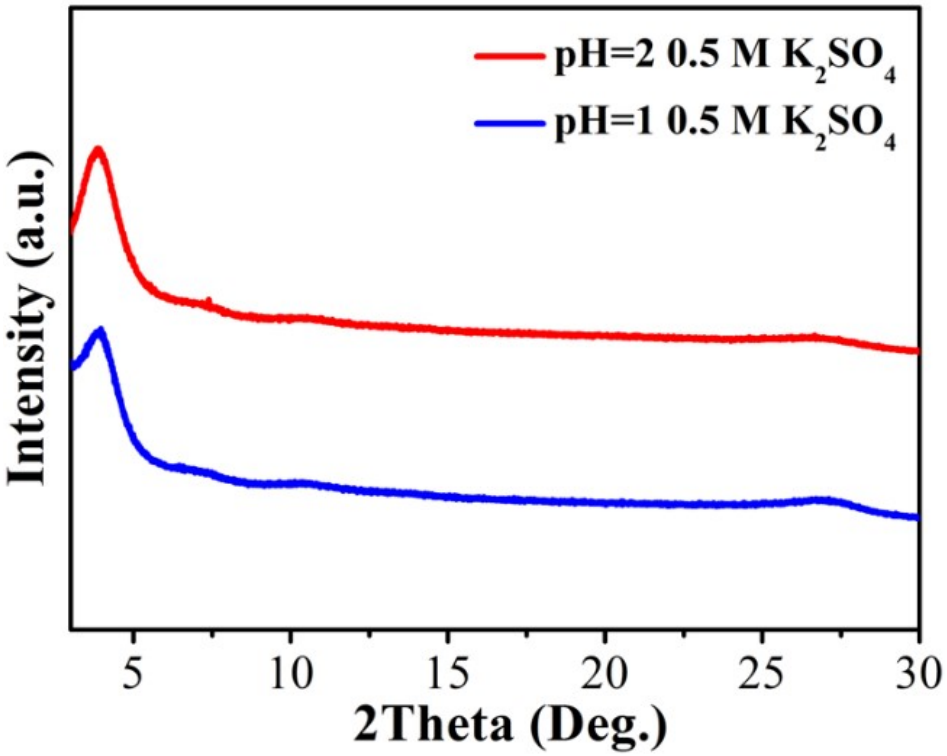

Figure S25. PXRD pattern of NiPc-Im-COF after electrocatalytic CO_2RR in 0.5 M K_2SO_4 (pH=1 and 2).

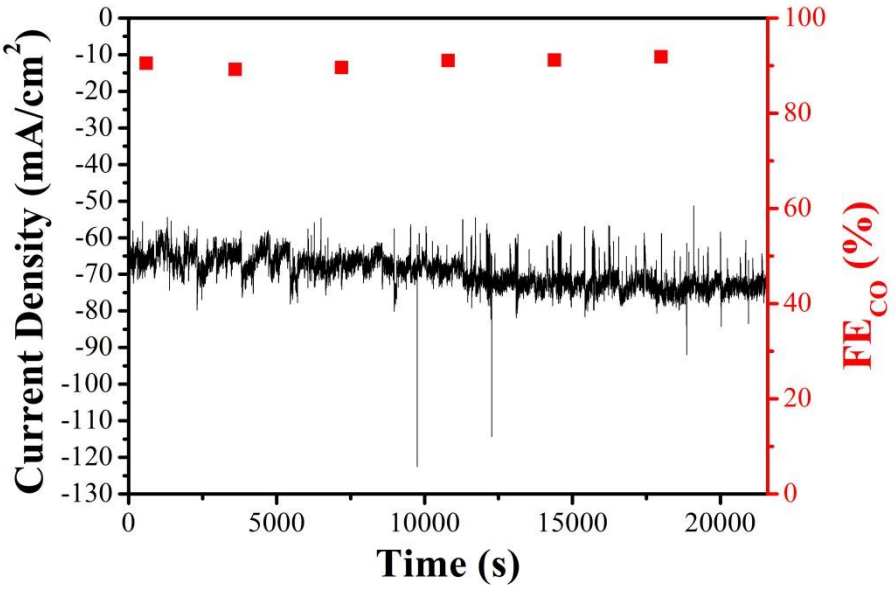

Figure S26. Long time stability test of NiPc-Im-COF at -1.3 V vs RHE in GDE with K_2SO_4 (pH = 1) as electrolyte.

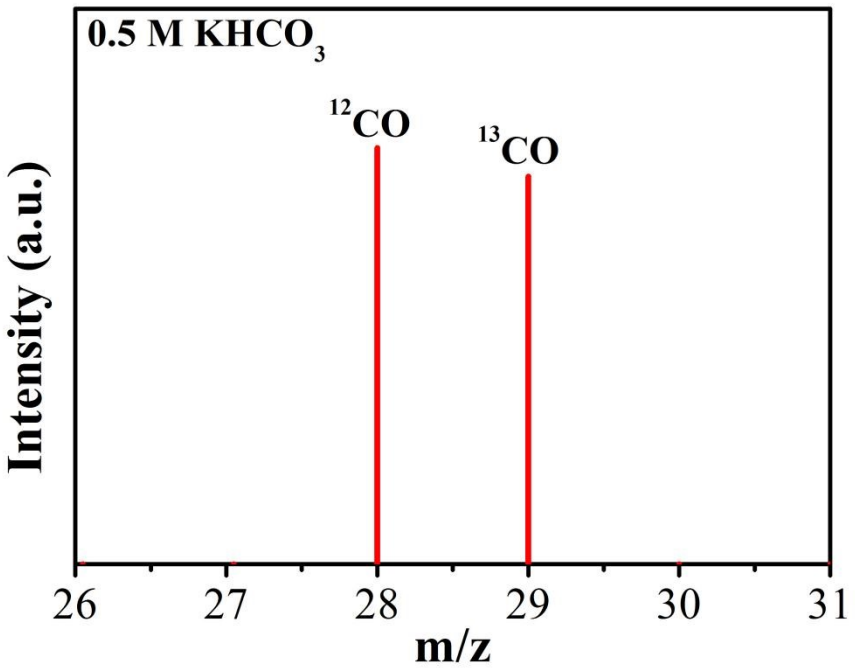

Figure S27. Mass spectra of CO in the $^{13}CO_2$-saturated 0.5 M $KHCO_3$ for NiPc-Im-COF.

Table S1. Result of Ni mass fraction measured by EDS.

Element	Mass fraction (wt/%)
Ni	3.59

Table S2. Results of C, N, H, Ni mass fraction measured by ICP.

Element	Mass fraction (wt/%)
Ni	3.75

Table S3. Porous characteristics of NiPc-Im-COF.

Sample	Slangmuir (m^2/g)	S_{BET} (m^2/g)	Total Pore Volume [cm^3/g]
Im-COF	699	360	0.32

Table S4. Parameters of the Ni K-edge EXAFS fitting results for NiPc-Im-COF.

Shell	**N**[a]	**σ^2 (10^{-3}Å^2)** [b]	**ΔE_0 (eV)** [c]	**R factor** [d]	**R (Å)** [e]
Ni-N	**4.2±0.60**	**3.7±2.4**	**5.29**	**0.053**	**1.84**

[a]N: coordination numbers; [b]σ^2: Debye-Waller factors; [c]ΔE_0: the inner potential correction. [d]R factor: goodness of fit; [e]R: distance between absorber and backscatter atoms; Fitting R-range = 1.0 - 2.3; Fitting k-range = 3 - 12.7.

References

1. M. Wang, M. Ballabio, M. Wang, H.-H. Lin, B. P. Biswal, X. Han, S. Paasch, E. Brunner, P. Liu, M. Chen, M. Bonn, T. Heine, S. Zhou, E. Cánovas, R. Dong and X. Feng, Unveiling Electronic Properties in Metal-Phthalocyanine-Based Pyrazine-Linked Conjugated Two-Dimensional Covalent Organic Frameworks, *J. Am. Chem. Soc.*, 2019, **141**, 16810-16816.
2. G. Kresse and J. Furthmiiller, Efficiency of ab-initio total energy calculations for metals and semiconductors using a plane-wave basis set, *Comput. Mater. Sci.*, 1996, **6**, 15-50.
3. G. Kresse, Efficient iterative schemes for ab initio total-energy calculations using a plane-wave basis set, *Phys. Rev. B*, 1996, **54**, 11169-11186.
4. G. Kresse and J. Hafner, Ab initiomolecular-dynamics simulation of the liquid-metal-amorphous-semiconductor transition in germanium, *Phys. Rev. B*, 1994, **49**, 14251-14269.
5. G. Kresse and J. Hafner, Ab initiomolecular dynamics for liquid metals, *Phys. Rev. B*, 1993, **47**, 558-561.
6. J. P. Perdew, K. Burke and M. Ernzerhof, Generalized Gradient Approximation Made Simple, *Phys. Rev. Lett.*, 1996, **77**, 3865-3868.
7. G. Kresse and D. Joubert, From ultrasoft pseudopotentials to the projector augmented-wave method, *Phys. Rev. B*, 1999, **59**, 1758-1775.
8. P. E. Blöchl, Projector augmented-wave method, *Phys. Rev. B*, 1994, **50**, 17953-17979.